Applied Catalysis B: Environmental 241 (2019) 41–51

Contents lists available at ScienceDirect

Applied Catalysis B: Environmental

journal homepage: www.elsevier.com/locate/apcatb

Renewable N-doped active carbons as efficient catalysts for direct synthesis of cyclic carbonates from epoxides and CO_2

Ajaikumar Samikannu[a,1], Lakhya Jyoti Konwar[a,1,*], Päivi Mäki-Arvela[b], Jyri-Pekka Mikkola[a,b]

[a] Technical chemistry, Department of Chemistry, Chemical-Biological Centre, Umeå University, SE-901 87 Umeå, Sweden
[b] Laboratory of Industrial Chemistry and Reaction Engineering, Johan Gadolin Process Chemistry Centre, Åbo Akademi University, Turku, FI-20500, Finland

ARTICLE INFO

Keywords:
CO_2 utilization
N-Doped carbons
Cyclic carbonates
Metal free catalysis

ABSTRACT

In the spirit of green chemistry and greenhouse gas mitigation, we explore herein the chemical utilization of CO_2 upon synthesis of cyclic carbonates over N-doped activated carbons. The N-doped carbocatalysts were obtained from inexpensive N-rich bio-waste precursors and characterized by standard techniques (N_2 physisorption, chemisorption, XPS, SEM, TEM, XRD, FT-IR and Micro-Raman spectroscopy). The materials exhibited excellent catalytic activity for direct carbonation of epoxides with CO_2 to cyclic carbonates (yields upto 99%) under solvent free, moderate temperature (100–150 °C) and low CO_2 pressure (5–50 bar) conditions. The observed catalytic activity of the N-doped carbocatalysts was attributed to the Lewis basic sites originating from pyridinic, pyridonic, and quaternary N-sites capable of activating the CO_2 molecule. While control experiments with multiwalled carbon nanotubes (MWCNT) or commercial activated carbon, failed to produce cyclic carbonates due to lack of active (basic) sites. In terms of the catalytic performance, the N-doped carbocatalysts presenting a high porosity (634–1316 m^2/g) and high levels of pyridinic (33%) and quaternary N-doping (30%), (i.e. CA500 and MA500), exhibited the highest activity and selectivity (TOF, conversion and cyclic carbonate yields upto 99% in 5–15 h). Most importantly, these materials demonstrated good operational stability and reusability.

1. Introduction

Inorganic CO_2 is the most long-lived greenhouse gas in earth's atmosphere and the root cause of global warming. Anthropogenic emissions from fossil fuel use and deforestation are recognized to be the main contributor to the increased atmospheric CO_2 levels, but large quantities of CO_2 are also obtained as a by-product from industrial processes such as steam reforming, ammonia synthesis, oil- and gas industry and fermentation. In view of these concerns, efforts have been made to reduce the atmospheric CO_2 level trough approaches such as shift to non-fossil/clean energy sources, CCS (carbon capture and storage) and CCR (carbon capture and recycling). Among them, the CCR or chemical fixation of carbon dioxide (CO_2) has gained considerable attention in recent years as CO_2 represents a renewable, virtually inexhaustible, nontoxic C1 building block and a potential substitute to hazardous reagents such as CO and phosgene [1,2]. Various methodologies have been developed for converting CO_2 into useful chemicals such as methanol, methane, dimethyl ether, formic acid, urea, methanol, formamidine derivatives, benzimidazole derivatives, cyclic carbonates and polycarbonates as well as pharmaceutical products [3]. Out of these, synthesis of cyclic carbonates and polycarbonates is at present considered as one of the most effective means of chemical CO_2 utilization (Scheme 1a). These carbonates are of significant industrial interest as solvents, electrolytes, lubricants, synthetic building blocks, fine chemicals, and as monomers for polymer synthesis [2,3]. The process involves, reacting epoxides with CO_2 at moderate temperatures (100 °C and above) and CO_2 pressures (upto 50 bar) in the presence of a catalyst (CO_2 is kinetically and thermodynamically stable and therefore a catalyst is needed to activate the molecule) [4]. Traditionally, cyclic carbonates are produced at industrial level from petroleum streams via transesterification of polyols with phosgene/phosgene reagents (e.g. di-*tert*-butyl dicarbonate, 1,1′-carbonyldiimidazole, and aromatic carbonates) (Scheme 1b) [5]. In addition to its toxicity, phosgene synthesis is energy intensive (from CO and Cl_2) and requires specialized safety and storage measures. Further, use of phosgene reagents also leads to unwanted side reactions, which renders downstream product recovery complicated and expensive [5,6]. Consequently, efforts have been made to develop green 'non-phosgene' routes for cyclicarbonate and Polycarbonates synthesis.

The most widely studied catalysts for carbonation of epoxides with

* Corresponding author.
E-mail address: lakhya07@gmail.com (L.J. Konwar).
[1] Equal contribution.

https://doi.org/10.1016/j.apcatb.2018.09.019
Received 4 July 2018; Received in revised form 27 August 2018; Accepted 8 September 2018
Available online 08 September 2018

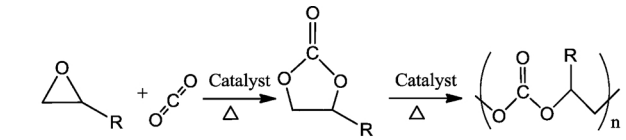

(a) green route based on direct carbonation of epoxides with CO_2

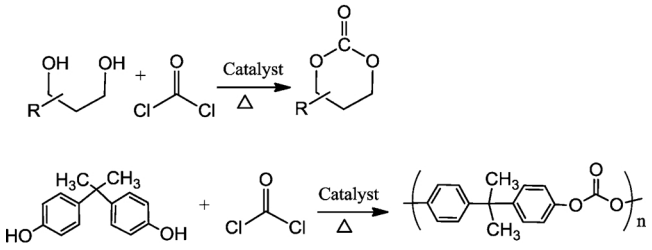

(b) traditional route based on phosgene/phosgene reagents

Scheme 1. Different routes for synthesis of cyclic carbonates and polycarbonates (a) direct carbonation of epoxides with CO_2 and (b) carbonation with phosgene/phosgene reagents.

CO_2 include transition metals, homogeneous metal complexes, phosphines, strong amine bases as well as ionic liquids [7–9]. Inspite, of the high catalytic efficiency under relatively mild conditions (< 150 °C and < 50 bar CO_2) use of these homogenous catalysts pose difficulties in downstream product recovery (high operational costs), catalyst separation and reusability issues which make continuous processing/industrial upscaling unrealistic.

Hence, there is a need to develop alternative approaches based on heterogeneous catalysts that are cheap, stable, recyclable, and efficient for the clean synthesis of cyclic carbonates. Accordingly, different solid bases and solid materials containing nucleophilic sites have also been explored as potential catalyst/co-catalyst for the cycloaddition of carbon dioxide, these include MgO, hydrotalcite (Mg–Al mixed oxide), KX zeolite, Cs-loaded KX zeolite, Cs-doped alumina, [10], supported amines [11], metal organic frameworks [12], graphitic carbon nitride [13], supported graphitic carbon nitride [14], graphene oxide [15], N-modified graphene oxide [16], Ionic liquid modified graphene oxide [17], polymers supported basic Ionic liquids [18] and very recently N-doped carbon materials [19,20]. Among, the solid catalysts the N-doped carbons are of particular interest as they represent a class of materials with all the features of an ideal heterogeneous catalyst (cheap, environmentally friendly, easy to synthesize and recyclable). However, further studies are needed in order to gain insights into the active sites, catalyst–substrate interactions and kinetic parameters upon the reactions catalyzed by N-doped carbons.

Keeping in mind the above points, in the present study, we have explored the catalytic potential of inexpensive biomass-derived N-doped activated carbons as metal free catalysts upon solvent free carbonation of epoxides with CO_2. The work was motivated by the recently recognized catalytic activity of N-doped carbon materials upon carbonation reaction and our group's recent works establishing the potential of nitrogen rich biomass wastes and polymers as efficient single precursors for the direct synthesis of versatile and highly porous N-doped carbon materials (9.8–16 at%) [21,22]. These materials have already been explored as electrocatalysts and catalyst supports upon many industrially relevant reactions [21–25]. The aim of the current work was to carry out a comprehensive study into the solvent-free carbonation of epoxides with CO_2 to cyclic carbonates over N-doped activated carbons in batch mode. The reactivity of different epoxides, catalyst composition and textural properties, initial CO_2 pressure, reaction temperature, kinetic aspects and reusability (stability of active sites) of N-doped active carbons are explored.

2. Experimental

2.1. Materials and methods

Glycidol (99%, Sigma-Aldrich), epichlorohydrin (99%, Sigma-Aldrich), propylene oxide (99%, Sigma-Aldrich), glycerol carbonate (99%, Sigma-Aldrich), methanol (99.9%, VWR), ethanol (95%, Merck), multiwalled carbon nanotubes (MWCNT, Sigma-Aldrich), active carbon (powder, fisher scientific) and phosphoric acid (85%, VWR) were obtained from commercial sources and used without further purification. The catalyst precursors were commercially available high molecular weight chitosan (Sigma-Aldrich) and non-food protein wastes (de-oiled seed waste cake, DOWC) obtained from *Jatropha curcas* and *Mesua ferrea* L. seeds after removal of oil by solvent extraction method (supplied by Department of Energy, Tezpur University, India).

2.2. Synthesis of N-doped carbon

The N-doped porous carbons were obtained by simple one step phosphoric acid activation of nitrogen containing biomass precursors (chitosan, *Jatropha curcas* and *Mesua ferrea* DOWCs) as described in our earlier works [23,24]. In a typical synthesis, 10 g of biomass (particle size < 250 μm) was mixed with 50% aqueous phosphoric acid solution in a 1:2 wt ratio and aged for 24 h under ambient conditions. In the next step, the aged biomass samples were transferred into ceramic crucibles and loaded into a muffle furnace (Nabertherm, LT15). Finally, the samples were activated at 500 °C for 1 h in the self-generated atmosphere to produce the doped carbon materials (heating rate was 2.8 °C/min). The resulting carbons were ground to powder (particle size < 100 μm) and thoroughly washed with hot deionized water (90 °C) until neutral pH, dried in an oven at 100 °C for 24 h and stored until further use (the yield of carbon materials was 35 ± 2%) [23]. The N-doped active carbon samples will be hereafter referred as CA500 (chitosan), JA500 (*Jatropha* DOWC based) and MA500 (*Mesua* DOWC based) respectively.

2.3. Catalyst characterization

The carbon materials were characterized by means of Infrared Spectroscopy (Bruker Vertex 80v FT-IR spectrometer with vacuum bench and DTGS detector), Raman spectroscopy (Renishaw InVia laser Raman microscope, 514.5 nm Ar-ion laser), X-ray Powder Diffraction (Bruker-AXS d8 Advance X-ray diffractometer using Cu Kα radiation. The elemental composition and oxidation state of surface functionalities were evaluated by X-ray photoelectron spectroscopy on a Kratos Axis Ultra DLD spectrometer with a monochromatized Al Kα X-ray source with charge neutralization operating at 14 kV, 300 W. The analyzer pass energy was 17.9 eV and the energy step was 0.1 eV. The vacuum chamber base pressure was10^{-9} mbar. The morphological features of the carbon materials were studied on a Carl Zeiss Merlin Field Emission Scanning Electron Microscope (FE-SEM) operating at 30 kV equipped with energy-dispersive X-ray spectroscopy (EDS, Oxford Instruments X-MAX 80 mm^2 X-ray Detector). Transmission electron micrographs (TEM) were recorded on a Jeol JEM-2100 electron microscope operating at 200 kV. The resolution was around 0.4 nm. Samples were suspended in ethanol and deposited on a copper grid for analysis. N_2 physisorption measurements were conducted on a Micromeritics TriStar 3000 porosimeter. Adsorption–desorption isotherms were recorded at −196 °C after the samples were outgassed at 150 °C for 3 h. The specific surface areas were calculated by the BET method and the pore volumes were calculated from desorption isotherms. The pore size distributions were estimated using the Barrett, Joyner and Halenda (BJH) algorithm (ASAP-2010) available as a built-in software from Micromeritics. Concentration of basic sites and the total amount of surface oxygen containing groups on carbon samples were determined by temperature-programmed-desorption (TPD) on a

Table 1
Surface and textural properties of catalytic materials utilized in the study.

Catalyst	Specific surface area	Pore volume	Pore diameter	[a]CO_2 basicity (mmol/g)			[b]Oxygen functional groups (mmol/g)	I_D/I_G	L_a
	(m^2/g)	(cm^3/g)	(nm)	total	weak	strong			(nm)
Activated carbon	1336	1.38	4.67	0.35	0	0.35	0.063	n.d	n.d
MWCNT	250	1.74	27	0	0	0	0	n.d	n.d
CA500	1316	0.93	2.7	0.485	0.015	0.47	0.059	0.86	5.08
JA500	251	0.29	4.67	0.666	0.022	0.644	0.11	0.85	5.17
MA500	635	0.46	3.77	0.457	0.015	0.442	0.062	0.73	6.02
JA500[c]	21	0.21	39.7	n.d	n.d	n.d	n.d	0.77	5.69
MA500[c]	210	0.22	4.03	n.d	n.d	n.d	n.d	0.70	6.25

[a] Based on CO_2-TPD.
[b] Total amount of oxygen containing surface functional groups determined from their decomposition by TPD.
[c] Catalyst recovered after 3rd reaction cycle.

BELCAT II instrument (MicrotracBEL Corp.). For basicity measurements CO_2 was used as probe (5% in He), in a typical measurement 50 mg sample was placed in an adsorption vessel and evacuated at 150 °C for 2 h under He flow. Then the sample was cooled to 50 °C in He flow. At this temperature, instrument grade CO_2 was passed through the sample for 1 h followed by heating to 80 °C in He flow for 1 h in order to remove physisorbed CO_2. TPD was carried out from 50 to 350 °C at a heating rate of 10 °C/min under He flow. After each measurement, the amount of CO_2 chemisorbed was determined form the calibration curve obtained from varying volumes of CO_2 in He. The total amount of oxygen containing surface functional groups on carbon samples were determined by their decomposition by TPD on the same instrument. In a typical measurement 50 mg sample was placed in an adsorption vessel and evacuated at 150 °C for 2 h under He flow. Then the sample was cooled to 50 °C in He flow. TPD was carried out from 50 to 350 °C at a heating rate of 10 °C/min under He flow. After each measurement, the total amount of surface oxygen containing groups was determined form the calibration curve obtained from varying volumes of CO_2 in He. The thermal stability of the catalytic materials were investigated by thermo gravimetric analysis (TGA 6000, PerkinElmer) from room-temperature to 800 °C at a ramping rate of 10 °C min^{-1} under N_2 flow (UHP grade).

2.4. Catalytic tests

The catalytic tests were performed in batch mode in a stainless steel mini autoclave with a capacity of 6.8 ml (the batch reactor was assembled from high pressure Swagelok fittings and equipped with a pressure indicator, emergency relief valve and digital temperature controller, Supporting information, Fig. S1). The reactor was heated on a sand bath and stirring was achieved magnetically with a stir-bar. In a typical reaction 20 mmol (ca. 1.16–1.85 g) epoxide (propylene oxide, glycidol and epichlorohydrin) and 100 mg catalyst (pre-dried @100 °C overnight) were loaded into the autoclave. In the next step, the reactor was flushed 5 times with instrument grade CO_2 (99.99%) to remove impurities and other reactive gases. Finally, the reactor was pressurized to the desired CO_2 pressure (5–50 bar) and the reaction mixture heated to the desired temperature (100–175 °C) for 0.5–15 h. To minimize the effect of intra-particle diffusion resistances of the reactants, small catalyst particles (particle size < 50 μm) and a vigorous stirring speed (400 rpm) was used in all experiments.

Upon completed reaction, the product from the autoclave was diluted with methanol (100 times) and analyzed by gas chromatography on an Agilent 6890 N instrument equipped with a HP-INNOWax column (30 m length, 0.25 mm internal diameter, and 1 μm of film thickness) and FID detector. Helium was used as the carrier gas. The GC injection port and the detector temperature were set at 250 °C. The following temperature programme was used for the analysis: initial column temperature was set at 100 °C for 1 min and programmed from 100 °C to 210 °C with the rate of 10 °C min^{-1} and held at this temperature for 10 min. Epoxide conversion and cyclic carbonate quantification were based on calibration curves obtained with standard compounds (epichlorohydrin carbonate was purified by vacuum distillation in order to obtain a calibration curve). The cyclic carbonate products were also confirmed by GC–MS (Agilent technologies model 5579 N) equipped with HP-5MS capillary column (30 m length, 0.25 mm internal diameter, 0.25 μm film thickness). The conversion and product selectivity are expressed as follows:

$$\text{conversion (mol \%)} = \frac{C_0 - C_t}{C_0} \times 100\,\% \quad (1)$$

$$\text{selectivity (mol \%)} = \frac{C_{carbonate}}{C_0 - C_t} \times 100\,\% \quad (2)$$

where, C_0 and C_t represent the concentration of epoxides (mol/L) at 0 h and t h, respectively, while and $C_{carbonate}$ represent the concertation (mol/L) of cyclic carbonate formed at the specified time. The catalyst turnover frequency (TOF) was expressed as:

$$TOF = \frac{k_{ini} \times C_{epoxide}}{n_{cat}} \quad (3)$$

where k_{ini} denotes the initial rate of carbonyl compound conversion, $C_{epoxide}$ the amount of carbonyl compound (in mmol) loaded into the reactor and n_{cat} the total amount of active sites (in mmol) on the catalyst loaded into the reactor.

3. Results and discussion

3.1. Catalytic material characterization

Table 1 summarizes the textural properties and structural parameters of as synthesized N-doped active carbons in comparison to commercial activated carbon and multiwalled carbon nanotubes (MWCNT) (reference catalysts). From the data, it can be seen that the N-doped activated carbons derived from biomass precursors (chitin and DOWCS) exhibited reasonably high porosity with a mixed meso and microporous structure. In fact, the specific surface area of CA500 (1316 m^2/g) was comparable to commercial active carbon (1336 m^2/g). In comparison the specific surface area of MA500 (635 m^2/g) and JA500 (251 m^2/g) were less than that of active carbon but higher than MWCNT (250 m^2/g). The average pore diameters of N-doped active carbons were in the range of 2.7–4.67 nm and also comparable to the commercial active carbon (4.67 nm). FE-SEM images revealed an irregular particle morphology for the N-doped activated carbons with visible cracks and defects (Fig. 1); TEM images also revealed a structure that was consistent with chemically activated amorphous carbon materials consisting of aromatic carbon sheets randomly stacked in all directions which gives rise to the characteristic textured morphology and porous structure (Fig. 1) [22,24]. The amorphous carbon structure (mixed sp2-sp3) of N-doped active carbons was further supported by the results of XRD and Laser Raman studies. The XRD patterns consisted

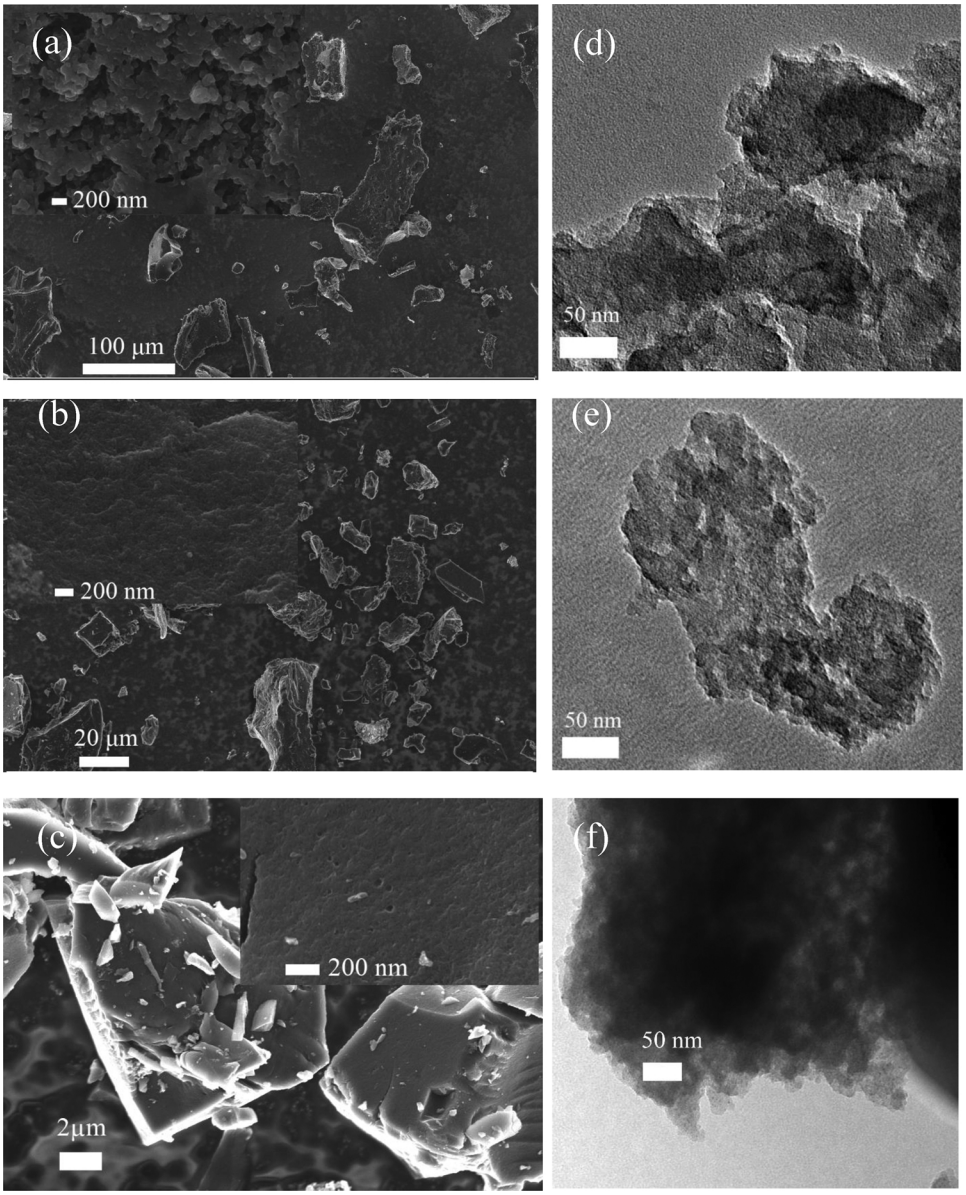

Fig. 1. SEM images of (a) JA500 (b) MA500 (c) CA500 and TEM images of (d) JA500 (e) MA500 (f) CA500.

of a broad (002) diffraction peak near 2θ = 15–30° and a very weak (101) graphitic structure peak near 2θ = 35–50° (data not shown). While, Laser Raman spectra (Fig. 2(a)) of the carbon samples showed two prominent peaks at 1350 cm^{-1} (D band) and ~1590 cm^{-1} (G band) along with a wide band extending from about 2550–3300 cm^{-1} (combination mode of D + G band) in consistent with a disordered carbon structure. The average graphitic cluster size (L_a) of the N-doped carbons were estimated from I_D/I_G intensity ratios ($I_D/I_G = C_\lambda/L_a$) and are summarized in Table 1 [24,26]. FT-IR analysis (Fig. 2(b)) also confirmed the amorphous carbon structure with surface oxygen functionalities indicated by the characteristic peaks of incompletely carbonized materials, near 1580 cm^{-1} and typical bands of carbonyl groups and hydroxyl groups, near 1700 cm^{-1} and 3500 cm^{-1}. Further, the existence of chemical bonding between carbon and nitrogen in the N-doped carbon structures was also supported by FT-IR patterns showing the stretching vibrations of C—N and C═N (1100–1600 cm^{-1}) groups (Fig. 2(b)) [21–24].

In terms of N-doping level, the order was as follows: CA500 > JA500 > MA500 > commercial active carbon = MWCNT according to the findings of XPS and EDX analysis, respectively (Table 2). EDX micro elemental mapping also revealed that these biowaste derived N-doped activated carbons presented a uniform, homogenous distribution of heteroatoms N and O (Figs. S2 and S3, Supporting information). The basicity values (concentration of basic sites) determined from temperature programmed desorption of CO_2 also followed a trend (JA500 > MA500 > activated carbon > MWCNT) that was consistent with level of heteroatom doping (N and O)/functionalization. The CO_2-TPD profiles (Fig. 2(c)) of N-doped carbons exhibiting strong desorption peaks near 110–120 °C and 240–340 °C were comparable to the TPD patterns reported by Guo et al. [27,28], and consistent with the presence of Lewis basic sites on the surface of N-doped active carbons containing pyridinic, pyridonic, and quaternary N species (Fig. 2(c) and Scheme 2). These desorption peaks were assigned to strong (240–340 °C) and weak (110–120 °C) basic sites respectively. The presence of Lewis basic sites on the N-doped carbons are further supported by the fact that in case of the reference carbocatalysts, no CO_2 desorption peaks were observed for MWCNT (in agreement with its non-functionalized structure); while a small 240–340 °C peak was recorded for commercial active carbon sample (assigned to the chemisorption of CO_2 on oxygen containing surface functional groups e.g.

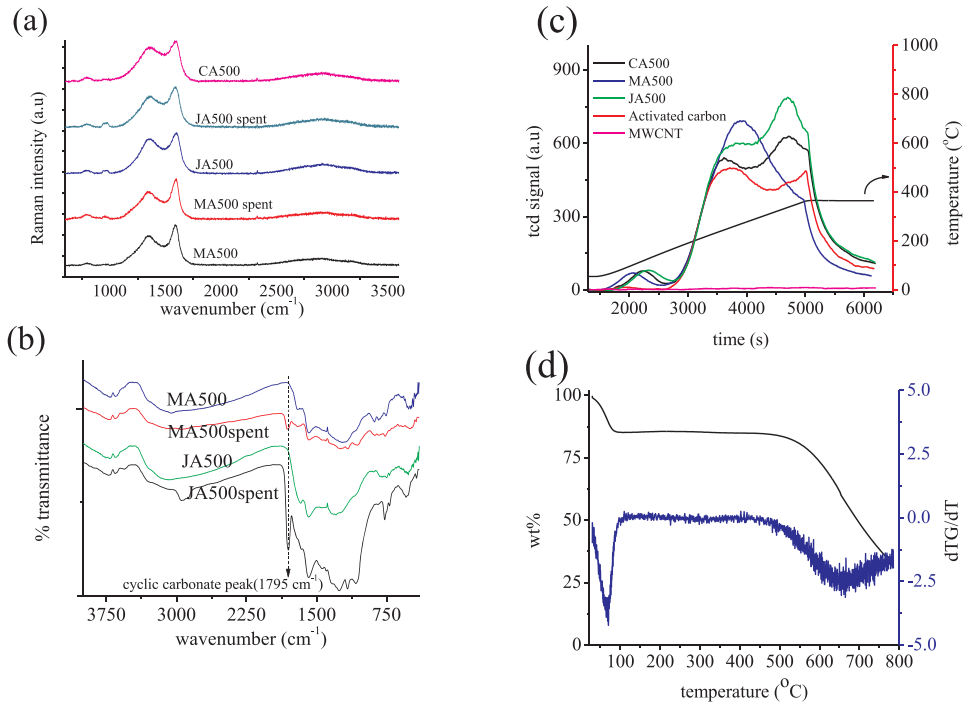

Fig. 2. (a) Laser Raman spectra, (b) FT-IR spectra (c) CO_2-TPD patterns and (d) TGA/DTA (shown for MA500) patterns of the N-doped carbocatalysts.

Table 2
Composition of N-species in the N-doped active carbons.

Sample	[a]Total N		% pyridinic N	% Pyrrolic & pyridonic N	% N quaternary	% N-oxide
	(wt%)	(at%)				
CA500	7.2	8.51	25	49.2	12.8	10.8
JA500	7.75	9.25	34.1	39.5	20.3	6.05
MA500	3.2	3.44	32.8	30.2	29.7	7.26
JA500[b]	2.25	2.72	21.32	72.05	6.62	0
MA500[b]	2.03	2.38	23.5	58.8	8.82	8.82

[a] Based on EDX.
[b] spent catalyst recovered after 3rd reaction cycle.

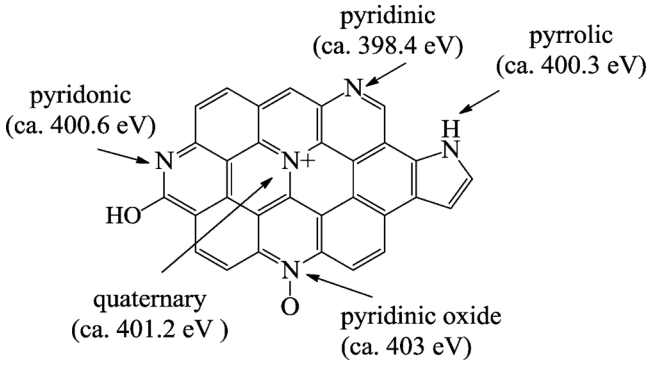

Scheme 2. The different possible configurations for nitrogen atoms in nitrogen-doped carbon materials.

lactones, carbonyls, phenols and −COOH as well as from their decomposition) [27,29]. The presence of surface oxygen functional groups on the carbon samples were also confirmed from the TPD evolution profiles of these samples, clearly showing peaks associated with decomposition of oxygen containing functional groups (release of CO and CO_2). The low temperature peak below 200 °C was attributed to the carboxylic groups while the high temperature peaks above 300–360 °C were attributed to lactone and phenolic groups (Fig. S4, supporting information). The difference in density of oxygen functionalities among the carbon materials also evident from the FT-IR results, with more functionalized carbon samples (JA500) clearly depicting sharper bands of carbonyl groups and hydroxyl groups (Fig. 2(b)).

The thermal properties of the carbocatalysts were investigated by thermogravimetric measurements under N_2 atmosphere (heating rate of 10 °C min^{-1}). Fig. 2(d) shows the TGA and DTA plots of a representative N-doped carbocatalyst MA500. It can be observed from the plots that only two weight loss event occurred in the carbocatalysts samples, the 1st weight loss region between 30–100 °C corresponded to the removal of moisture and trapped gases while the 2nd and more rapid weight loss region between 450–800 °C could be assigned to the further carbonisation/ graphitization of the material with removal heteroatoms (O, N) in the form light gases (CO, CO_2, NO_2 and H_2O). Consequently, from the thermogravimetric studies the operational stability of the N-doped carbocatalysts were approximated to be ~450 °C. These findings were comparable to the trends typically reported in literature [19–24].

The XPS results were in strong agreement with the CO_2-TPD results, the deconvolution of N1s XPS peaks of N-doped active carbons confirming the presence of serval N-species (pyridinic, pyrrolic, pyridonic, quaternary and N-oxide of pyridinic N) Fig. 3(a and b) [20–2527]. Similar, to the N-doped carbon materials reported in literature, the peak centred at 398.4 eV was associated to the presence of pyridinic N, while the peaks at 400.3–400.6 eV, 401.2 eV and 403 eV were ascribed to pyrrolic/pyridonic, quaternary and N-oxide of pyridinic N, respectively (Scheme 2). Even so, significant differences could be observed in the composition of N-species in the biomass derived N-doped activated carbons, most importantly MA500 presented ca. 10% higher quaternary-N (reported to be the most active N-species for CO_2 activation) as compared to JA500 (Table 2) whereas CA500 presented the highest percentage (49%) of pyrrolic/pyridonic N [22,24,27]. Similarly, the C1s XPS peak was resolved into five components (Fig. 3(c and d)) the largest peak at 284.3 eV was assigned to the sp2-hybridized graphite-like carbon(C−C sp2), the peak at 285.7–286 eV was assigned to the overlapping signal of C−N and C−O sp2 carbon, the peak centred at 287 eV and 289.2 eV were attributed to the C═O and O−C═O corresponding to the various oxygen functional groups on the material

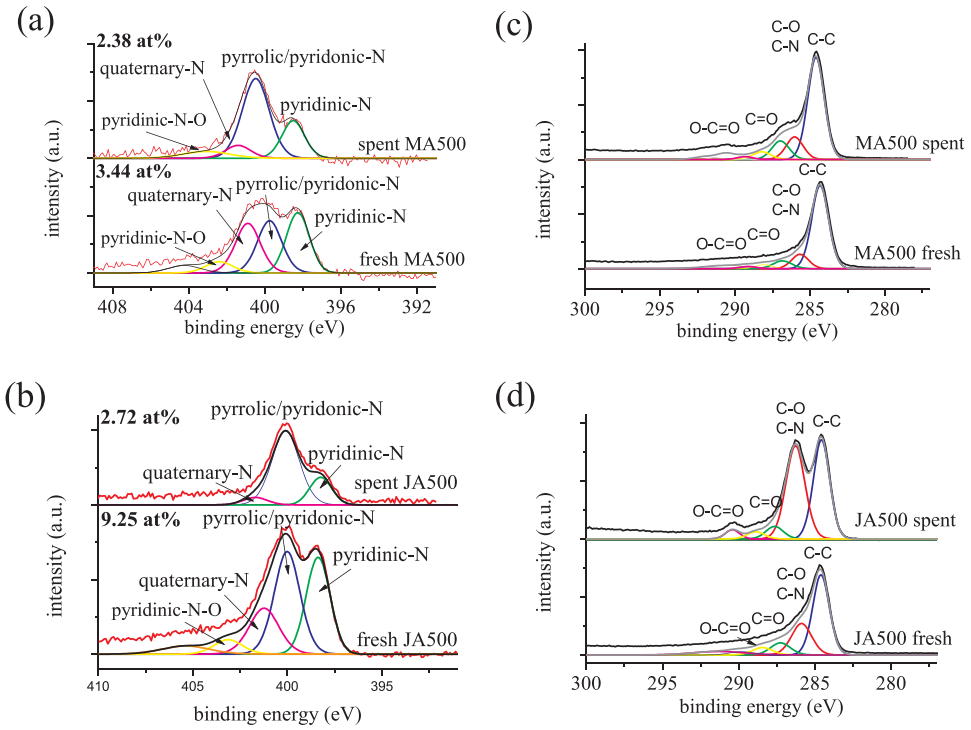

Fig. 3. High resolution (a) N1s and (b) C1s XPS spectra of carbocatalysts (spectra shown for representative carbocatalysts MA500 and JA500 before and after reuse during epichlorohydrin epoxidation).

surface [20–25,27]. However, when comparing the C1s and N1s peaks of spent and fresh N-doped carbocatalysts some significant changes could be observed (particular for JA500). The increased intensity observed for the pyrrolic/pyridonic in the N1s spectra and increased intensity of C—N/C—O sp2 carbon, C═O and O—C═O peaks in C1s spectra of spent catalyst could be attributed to the poisoning of carbocatalyst surface with strongly chemisorbed organic molecules (reactants and product molecules) [22,24,27]. An elaborate discussion on the mechanism of catalyst deactivation is given in Sections 3.2.3 and 3.2.4.

3.2. Catalytic activity

3.2.1. Results of initial catalytic tests upon carbonation of epoxides with CO_2

Table 3 summarizes the results of preliminary catalytic tests conducted with the different carbocatalysts upon solvent free carbonation of epichlorohydrin at 150 °C and 15 bar CO_2 in comparison to the reference homogeneous catalyst pyridine. The data presented in Table 3 clearly show that with respect to epichlorohydrin conversion and cyclic carbonate yield, only N-doped carbons were catalytically active, while the reference non-doped carbocatalysts (commercial activated carbon and MWCNT) were unsuccessful in catalyzing the reaction (no cyclic carbonate formation and conversions comparable to blank experiments). The inability of activated carbon and MWCNT to catalyze reaction was attributed to the lack of basic sites capable of activating CO_2 (clearly evident in CO_2-TPD and XPS results, Figs. 2 and 3). As expected, the initial rate of epichlorohydrin conversion for the solid catalysts followed the trend CA500 > MA500 > JA500 > active carbon > MWCNT in agreement with the combined effects of catalyst porosity and basicity; while TOF of epichlorohydrin conversion was in the order CA500 > MA500 > pyridine > JA500 > active carbon > MWCNT. In fact, the activity (TOF) observed for two of the carbocatalysts (CA500 and MA500) were almost three folds higher the reference homogeneous catalyst pyridine confirming the catalytic potential of N-doped carbons for carbonation of epoxides. In terms of desired product selectivity (cyclic carbonate), among the N-doped carbons, epichlorohydrin carbonate selectivity reached upto 99 mol% over MA500 catalyst (same as pyridine) while for JA500 and CA500 it was 93% and 94%, respectively in 15 h. The reduced selectivity (less than stoichiometric yield) was found to be mainly associated with the strong chemisorption of cyclic carbonates by the oxygen functionalities present on carbocatalyst surface and to some extent due to the formation of decomposition products (see below). Most importantly, no-side products or polymeric by-products could be detected upon the reactions catalyzed by carbocatalysts.

Table 3
Results of preliminary catalytic tests conducted with the different catalysts upon carbonation of epichlorohydrin with CO_2.

Catalyst	Initial rate (h^{-1})	Turnover frequency (h^{-1})	[a]Conversion (%)		[a]Cyclic carbonate selectivity (%)	
			5 h	15 h	5 h	15 h
Blank	0.001	–	0	2	0	0
Pyridine*	2.76	242	99	–	> 99	–
Activated carbon	0.013	7.5	0	18	0	0
MWCNT	0.0013	–	0	2.5	0	0
CA500	1.74	718	97	> 99	87	94
JA500	0.32 (0.15)	93.3 (45)	72	> 99	86	93
MA500	1.55 (1.31)	680 (573)	88	> 99	98.8	98.5

Figures in parentheses () represent values for spent catalyst.
[a] Conditions: 100 mg catalyst (*equivalent to amount of N-sites in MA500), 20 mmol epichlorohydrin, 15 bar CO_2, 150 °C, 400 rpm stirring rate.

3.2.2. Investigation of N-doped carbons as a catalyst upon carbonation of epoxides with CO_2

Motivated by the promising results, in order to understand the effects of surface and textural properties on the catalyst reactivity and selectivity, the N-doped activated carbons MA500 (high performing)

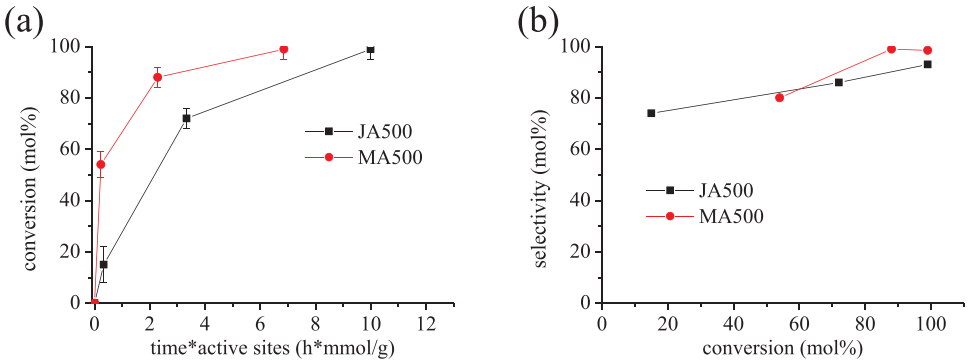

Fig. 4. (a) epichlorohydrin conversion vs normalized time (time*active sites) (b) conversion vs. cyclic carbonate selectivity. Conditions: 100 mg MA500, 20 mmol epichlorohydrin, 150 °C, 15 bar CO_2, 400 rpm stirring rate.

and JA500 (low performing) were further evaluated for optimization, kinetic and reusability studies upon carbonation of different epoxides with CO_2. Fig. 4(a) shows the plots of epichlorohydrin conversion as a function of normalized time (time*active sites) over the two N-doped carbocatalysts while Fig. 4(b) shows epichlorohydrin carbonate selectivity as function of normalized conversion. The conversion trends were found to be consistent with the initial rate/TOFs values presented in Table 3 and confirms the superiority of MA500 (and also CA500) over JA500. From selectivity vs. conversion plots it could be seen that cyclic carbonate selectivity never reached its theoretical value (100%) although no by byproducts were formed under the reaction conditions. The reduced selectivity which contributed to a less than stoichiometric cyclic carbonate yield, could be attributed to the strong chemisorption of oxygenated product molecules (organic cyclic carbonates) on the oxygen functionalities and basic (active) sites present on the surface of N-doped carbocatalysts. The effect was more noticeable at lower conversion levels particularly for JA500 (76% product selectivity at 20% conversion) when the concentration of organic carbonates was considerably lower. The chemisorption of organic carbonates was more prominent for JA500 (as well as CA500) due to its surface structures constituting a higher density of basic sites (~1.4 fold higher) and oxygen functional groups (~1.7 fold higher) when compared to MA500 catalyst (Table 3). This chemisorption effect also contributed to deactivation/poisoning of the carbocatalysts, a detailed discussion on the chemisorption and mechanism of catalyst deactivation is given in Section 3.2.4 (see below). Also, comparison of the activity trends observed for the different carbocatalysts with the amount surface oxygen functionalities (OH and COOH groups) and basicity showed a synergetic effect of similar to the trends found in literature [17]. Overall, the catalytic activity of the carbocatalysts were governed by the combined effects of concentration of surface basic sites, oxygen functionalities and porosity surface (Tables 1 and 3). Table S1 (Supporting information) gives a comparative overview of the catalytic activity bio-waste derived N-doped activated carbons with the N-doped carbons reported in literature [19,20].

Fig. 5(a) shows the effect of initial CO_2 pressure on epichlorohydrin conversion and Fig. 5(b) epichlorohydrin carbonate yield. The positive correlation observed between rate of carbonation and cyclic carbonate yield with increasing initial CO_2 pressure in Fig. 4 were consistent with an equilibrium driven pseudo 1st order reaction mechanism and in agreement to the trends reported in literature for carbonation of epoxides [19,20,30,31]. Overall, an initial CO_2 pressure of 15 bar was found to be optimum as 5 bar CO_2 was not adequate to reach desirable conversions (≥90 mol%) even after 15 h. The effect of reaction temperature is illustrated in Fig. 6(a) shows that with increasing temperature the rate of carbonation as well as yield of epichlorohydrin carbonate increases, reaching its maximum value at 150 °C. The use of higher reaction temperatures ≥175 °C resulted in reduced cyclic carbonate selectivity due to formation of epoxide/cyclic carbonate decomposition products (3-chloro-2-hydroxypropyl formate and 3-chloropropane-1,2-diol via thermal ring opening) as well as polymeric self-condensation products of organic carbonates. However, it should be noted that use of temperatures lower than 125 °C resulted in very slow reaction rates and consequently, 150 °C was considered to be the optimum reaction temperature for carbonation of epoxides with N-doped active carbon catalysts (all reusability studies conducted at this temperature). Using the pseudo 1st order rate constants the Arrhenius plot (ln k versus 1/T) were obtained (Fig. 6(b)). Using these plots, the activation energy (E_a) of reaction was estimated to be 39.6 kJ/mol and 43.3 kJ/mol for MA500 and JA500, respectively. The E_a value ($E_a > 25$ kJ mol^{-1}) indicated that under the investigated conditions the reaction was kinetically controlled and not limited by inter-particle diffusion or external mass transfer limitations [31]. It should also be noted here that under the investigated reaction conditions, the contribution from autocatalysis was negligible as the rate of the unanalyzed (bank reaction) was at least 10 times lower than the catalyzed reactions.

Experiments were also conducted to probe the reactivity of different

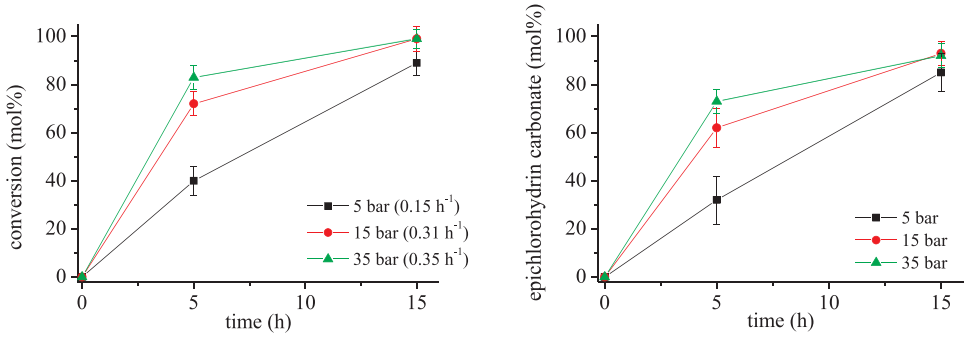

Fig. 5. The influence of initial CO_2 pressure on (a) epichlorohydrin conversion (represent initial rates) and (b) yield of epichlorohydrin carbonate. Conditions: 100 mg JA500, 20 mmol epichlorohydrin, 150 °C, 400 rpm stirring rate.

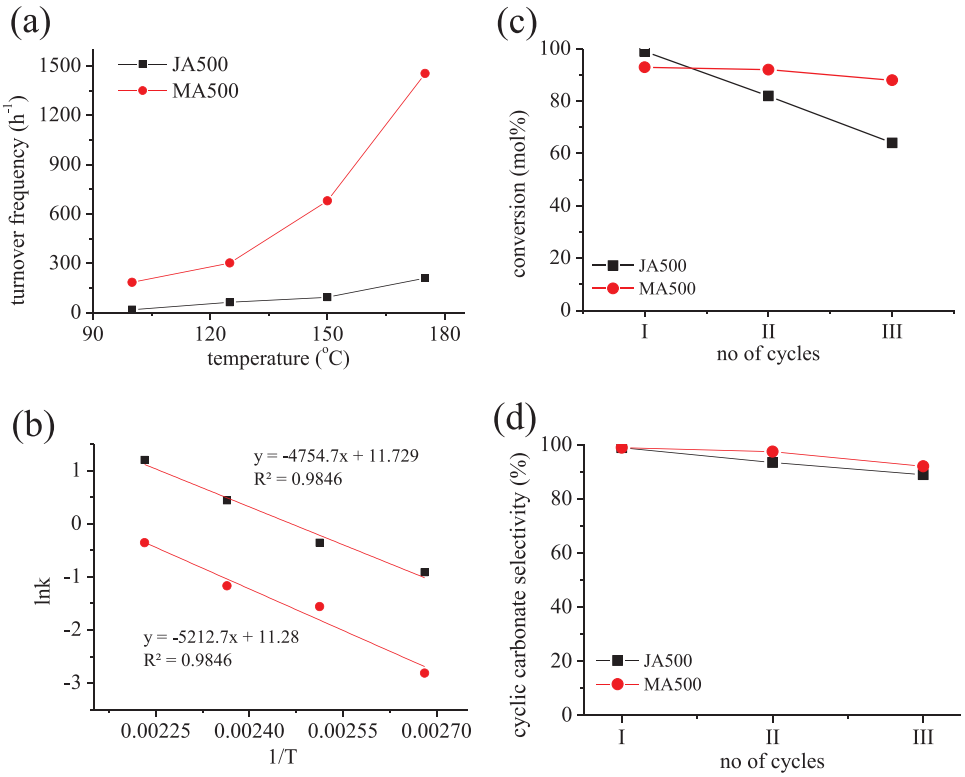

Fig. 6. (a) Turnover frequency (h^{-1}) vs. reaction temperature, (b) Arrhenius plot (ln*k* vs. 1/T), (c) epichlorohydrin conversion vs. reuse and (d) epichlorohydrin carbonate selectivity vs. reuse. Conditions: 100 mg catalyst, 20 mmol epichlorohydrin, 150 °C (c and d), 400 rpm stirring rate.

Table 4
The influence of epoxide on catalytic performance of N-doped activated carbons.

Catalyst	epoxide	TOF (h^{-1})	[a]Conversion (%)	[a]Cyclic carbonate selectivity (%)
J500	epichlorohydrin	93.3	99	93
	glycidol	90	99	94
	propylene oxide	3	15	80
M500	epichlorohydrin	680	99	99
	glycidol	642	99	99
	propylene oxide	7 (*38)	30 (*84)	89 (*98.5)

[a] Conditions: 100 mg catalyst, 20 mmol epoxide, 150 °C, 15 bar CO_2 (*50 bar), 15 h (*24 h), 400 rpm stirring rate.

epoxides upon CO_2 carbonation with the N-doped activated carbon catalyst. Table 4 summarizes the results carbonation experiments conducted with different epoxides (epichlorohydrin, glycidol and propylene oxide) using the N-doped carbocatalysts JA500 and MA500 at 15 bar initial CO_2 pressure. The data (TOF and initial rate) presented in Table 4 indicated that the epoxides with electron withdrawing groups (epichlorohydrin, glycidol) were more reactive (higher TOF, conversion approaching ~99% in 15 h), while propylene oxide (with electron donating alkyl substituent) was significantly less reactive (only 15 mol % conversion in 15 h). The cyclic carbonate selectivity was ≥93 mol% for epichlorohydrin and glycidol whereas in case of propylene oxide it was only 80 mol%. Nonetheless, practical conversions (~84 mol%) could be obtained for the less reactive propylene oxide with by increasing the initial CO_2 pressure (50 bar) and reaction temperature, in agreement with the equilibrium driven reaction mechanism of epoxide carbonation [17,18,30,31]. The selectivity to propylene carbonate was 99 mol%. The overall order of epoxide reactivity based TOF values was epichlorohydrin > glycidol > propylene oxide for both catalysts.

3.2.3. Plausible reaction mechanism

Based on the experimental results obtained in the current work and previously published results, a plausible mechanism was proposed for the carbonation of epoxides with CO_2 over the N-doped carbocatalysts (Scheme 3). The reaction may be closely approximated by a Lewis-base (pyridine, guanidine) catalyzed mechanism [9,30,32,33], with the basic pyridinic, pyridonic and quaternary N acting as the active site for CO_2 activation and cyclic carbonate formation. The reaction begins with the (a) adsorption/activation of CO_2 on the Lewis-basic sites (step 1) and (b) epoxides on the oxygen functional groups (−COOH and −OH) of N-doped carbon (I) forming the activated catalyst (II). In the second step epoxides are desorbed and CO_2 is inserted into the C−O bond of epoxide via a nucleophilic attack forming the activated complex III. In the final step (step 4) the cyclic carbonate molecule is formed via an intramolecular nucleophilic attack, simultaneously the active sites are also for vacated next reaction cycle. However, the synergetic effects among hydroxyl group and basic site is very important in these materials, a high-density oxygen functional groups can also contribute to reduced catalytic activity due to the poisoning of catalyst surface by the strongly chemisorbed oxygenated molecules such as epoxides and cyclic carbonates (Supporting information, Fig. S5) [34–36].

3.2.4. Reusability and spent catalysts characterization

Finally, reusability studies were conducted with MA500 and JA500 in order to investigate the operational stability of N-doped carbocatalysts upon carbonation of epoxides with CO_2. The catalyst particles recovered/regenerated by centrifugation, thorough washing with methanol, deionized water and oven drying (100 °C, 24 h) were re-evaluated upon epichlorohydrin carbonation under optimized conditions (15 bar, 150 °C). The reusability data presented in Fig. 6(c) showed that among the two carbocatalysts, JA500 showed a more rapid and noticeable ~40% loss of catalytic activity while MA500 could maintain 90% of its original activity during three successive reaction cycles. As expected, the reduced catalyst activity was also accompanied with

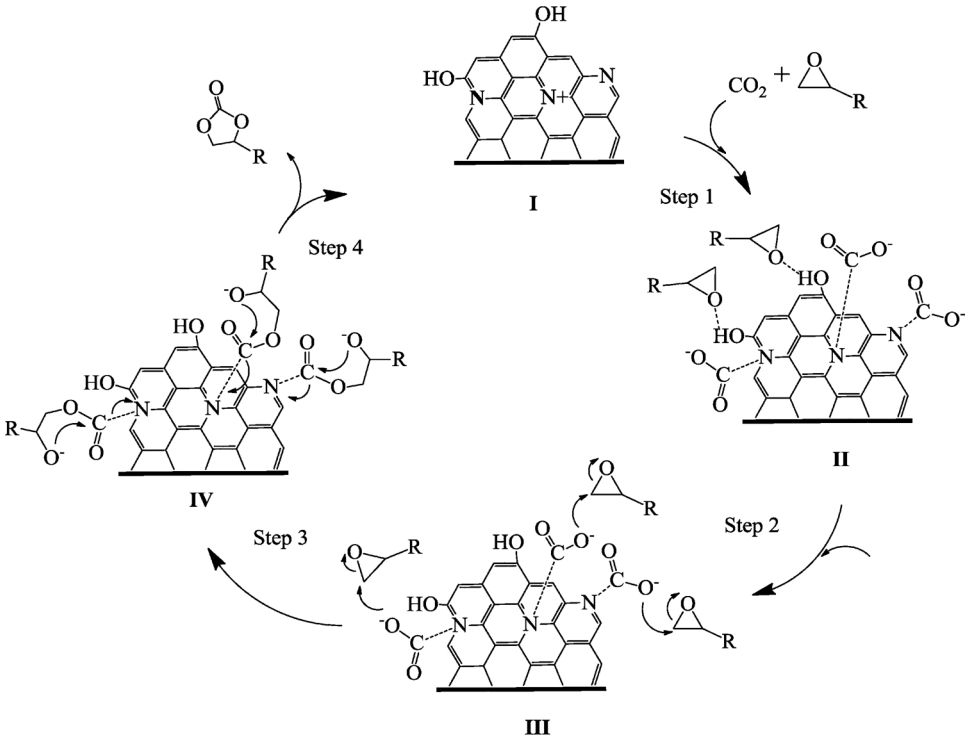

Scheme 3. Plausible mechanism depicting the carbonation of epoxides with CO_2 to cyclic carbonates over N-doped activated carbons.

reduced of cyclic carbonate yield, which was also more pronounced for the carbocatalyst JA500 (ca 5%) (Fig. 6(d)). The reduced catalyst performance and superior stability of MA500 was also evident from the kinetic parameters of spent carbocatalysts presented in Table 3, which showed that initial rate and TOF reduced by 15% percent during the 1st recycle of MA500 whereas for JA500 the initial rate and TOF dropped by almost 50%. Our results are drastically different from previous studies which have demonstrated the good reusability of similar N-doped carbocatalysts (only 3–5% loss in conversion/activity) [17,18].

Thus, in order to explain our findings and understand the mechanism/cause of catalyst deactivation we took a more comprehensive approach and studied the structural and chemical changes that occurred on the surface catalytic materials during the reaction/reaction cycles by characterizing the spent catalyst particles through techniques such as FT-IR, N_2-physisorption, laser Raman spectroscopy and XPS. Comparison of the characterization results of spent catalyst particles with fresh catalytic materials revealed major changes to the surface chemistry, structural and textural properties of spent JA500 and MA500 catalysts (Table 1, Figs. 2 and 3). The N_2-physisorption data presented in Table 1 shows that specific surface area of spent JA500 and MA500 reduced to 21 and 210 m^2/g from 251 and 634 m^2/g, respectively during three reaction cycles resulting from the strong chemisorption of organic molecules (epoxides and cyclic carbonates) (Scheme 4(a)). The chemisorption of organic molecules were supported by the results of micro Raman spectroscopy showing increased graphitic cluster size (Table 1 and Fig. 2(a)) and FT-IR spectra appearance of the characteristic peaks of organic cabonates and epoxides in the spent catalysts (Fig. 2(a)). XPS (Fig. 3) and elemental analysis (Table 2) provided further confirmation on the changes in surface chemistry and composition of the spent carbocatalysts; the results of elemental analysis/XPS showed that for spent JA500 catalyst recovered after three reaction cycles the N-doping level reduced to 30% of the original while for spent MA500 it reduced to 70% of the original material. However, the altered bulk chemical composition (reduced N-doping and increased O doping) is not due to leaching but is a consequence of adsorption oxygenated molecules on the material surface (supported by the increased mass and reduced porosity of spent catalyst). Further, comparison of the high resolution N1s spectra of the fresh carbocatalysts with the spent carbon materials showed that upon reuse changes also occurred in the chemical composition of N-species; ~27–33% increase in the amount of pyridonic-N (ca. 400.6 eV) with ~14–21% and ~10–13% decrease in quaternary-N (ca. 401.2 eV) and pyridinic-N (ca. 398.4 eV), respectively (Fig. 3(a and b)). We believe that such compositional change in the N-species occurs via an oxidative mechanism (Scheme 4(b)), where oxygen/O sites are most likely supplied from the carbon surface or the reactants, similar to the transformation of pyridinic-N during oxygen reduction reactions (ORR) and also contributed partially to the poisoning of catalysts [28]. The increased intensity of C—N/C—O sp2 carbon, C═O and O—C═O peaks in C1s spectra of spent catalyst also support the chemisorption of epoxides and organic carbonates (Fig. 3(c and d)) [22,24,27]. The chemisorption effect leading to poising was more pronounced over the JA500 catalyst which presented a ~2.6 fold higher levels of N-doping and ~1.7 fold higher oxygen functional group density than MA500. The higher level of N-doping coupled with high density of oxygen functional groups translated to an increased CO_2 basicity (~1.4 fold higher density of basic sites) and surface hydrophilicity which aided stronger chemisorption of oxygenated molecules like cyclic carbonates, epoxides as well as CO_2 thereby contributing to the fast and irreversible poisoning of JA500 carbocatalyst [34–36]. This stronger chemisorption effect of JA500 was also evident in the FT-IR and C1s XPS spectra of spent JA500 catalyst. These characterization results also confirm that the reduced cyclic carbonate selectivity and less than stoichiometric yield observed with the N-doped carbocatalysts are indeed due to chemisorption of product on catalyst surface. These findings suggested that a high porosity and moderate level of N-doping are most important parameters for obtaining a highly active, reusable carbocatalyst for direct carbonation of epoxides. Further, studies are underway to address the above issues by tuning catalyst surface chemistry and reduce catalyst poisoning for application in a fixed bed rector.

4. Conclusions

In conclusion, inexpensive biomass derived N-doped activated

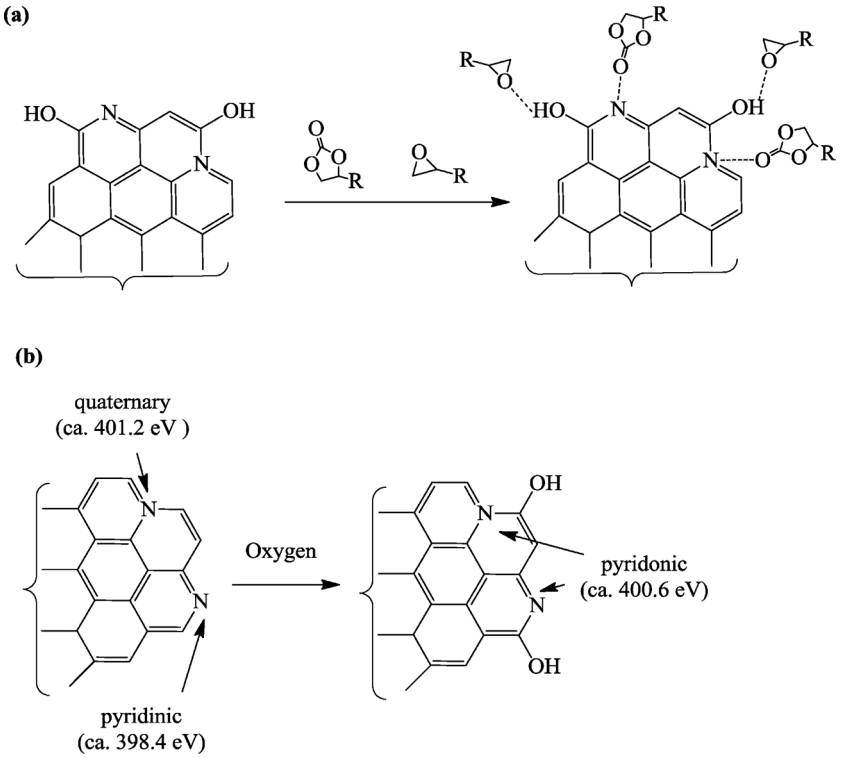

Scheme 4. Plausible mechanisms for the deactivation of N-doped carbocatalyst (a) deactivation by chemisorption of oxygenate molecules and (b) oxidative transformation of active N-sites.

carbons were demonstrated as catalysts in the synthesis of cyclic carbonates from direct carbonation of epoxides (epichlorohydrin, glycidol and propylene oxide) with CO_2. The N-doped activated carbons with a high porosity and CO_2 basicity exhibited excellent catalytic activity for CO_2 activation and conversion, in contrast the un-doped carbocatalysts viz. activated carbon and MWCNT were inactive. The carbon materials catalyze the direct carbonation of epoxides with CO_2 to cyclic carbonates (yields upto 99%). The catalytic activity of the N-doped carbocatalysts originated from the Lewis basic pyridinic, pyridonic, and quaternary N-sites. The optimum carbocatalysts (MA500 and CA500) exhibited 3 fold higher activity than that of pyridine under solvent free conditions without use of any co-catalysts/modifiers. Most, importantly the N-doped carbocatalysts exhibiting a high specific surface area and low density of oxygen functional groups (MA500) could be reused without any noticeable change in activity and selectivity.

Acknowledgments

Kempe Foundations (Kempestiftelserna), the Bio4Energy programme and Wallenberg WoodScience Center (WWSC) are gratefully acknowledged. Kempe Foundation is also acknowledged for providing postdoctoral fellowship to Lakhya Jyoti Konwar at Umeå University. The authors acknowledge the facilities of Umeå Core Facility Electron Microscopy (UCEM) and technical assistance of Dr. Cheng Choo Nikki LEE at the Chemical Biological Centre (KBC), Umeå University. This work is also a part of the Johan Gadolin Process Chemistry Centre.

Appendix A. Supplementary data

Supplementary material related to this article can be found, in the online version, at doi:https://doi.org/10.1016/j.apcatb.2018.09.019.

References

[1] T. Ema, K. Kukuhara, T. Sakai, T. Ohbo, F.-Q. Bai, J.-Y. Hasekawa, Catal. Sci. Technol. 5 (2015) 2314–2321.
[2] T. Sakakura, J.C. Choi, H. Yasuda, Chem. Rev. 107 (2007) 2365–2387.
[3] H.B. Lars, L. Johannes, S.C. Wulf, T. Werner, Top. Curr. Chem. (Z) 375 (2017) 50.
[4] B.R. Buckley, A.P. Patel, K.G.U. Wijayantha, RSC Adv. 4 (2014) 58581–58590.
[5] H.-J. Buysch, Carbonic esters, Ullmann's Encyclopedia of Industrial Chemistry, Wiley-VCH, Weinheim, 2005, https://doi.org/10.1002/14356007.a05_197.
[6] M. Taherimehr, P.P. Pescarmona, J. Appl. Polym. Sci. 131 (2014) 41141, https://doi.org/10.1002/APP.41141.
[7] R.L. Paddock, S.T. Nguyen, J. Am. Chem. Soc. 123 (2001) 11498–11499.
[8] J.W. Huang, M. Shi, J. Org. Chem. 68 (2003) 6705–6709.
[9] W.-L. Dai, S.-L. Luo, S.-F. Yin, C.-T. Au, Appl. Catal. A Gen. 366 (2009) 2–12.
[10] M. Tu, R.J. Davis, J. Catal. 199 (2001) 85–91.
[11] A. Barbarini, R. Maggi, A. Mazzacani, G. Mori, G. Sartori, R. Sartorio, Tetrahedron Lett. 44 (2003) 2931–3048.
[12] O.V. Zalomaeva, A.M. Chibiryaev, K.A. Kovalenko, O.A. Kholdeeva, B.S. Balzhinimaev, V.P. Fedin, J. Catal. 298 (2013) 179–185.
[13] D.-H. Lan, H.-T. Wang, L. Chen, C.-T. Au, S.-F. Yin, Carbon 100 (2016) 81–89.
[14] Z. Huang, F. Li, B. Chen, T. Lu, Y. Yuan, G. Yuan, Appl. Catal. B: Environ. 136–137 (2013) 269–277.
[15] D.-H. Lan, F.-M. Yang, S.-L. Luo, C.-T. Au, S.-F. Yin, Carbon 73 (2014) 351–360.
[16] D.-H. Lan, L. Chen, C.-T. Au, S.-F. Yin, Carbon 93 (2015) 22–31.
[17] D.-H. Lan, Y.-X. Gong, N.-Y. Tan, S.-S. Wu, J. Shen, Carbon 127 (2018) 245–254.
[18] D. Wei-Li, J. Bi, L. Sheng-Lian, L. Xu-Biao, T. Xin-Man, A. Chak-Tong, Catal. Sci. Technol. 4 (2014) 556–562.
[19] X. Ma, B. Zou, M. Cao, S.-L. Chen, C. Hu, J. Mater. Chem. A 2 (2014) 18360–18366.
[20] R.A. Molla, A. Iqubal, K. Ghosh, M. Islam, ChemistrySelect 1 (12) (2016) 3100–3107.
[21] L.J. Konwar, New Biomass Derived Carbon Catalysts for Biomass Valorization, ISBN 978-952-12-3395-1 (print), ISBN 978-952-12-3396-8 (PDF) Åbo Akademi University, Painosalama Oy) Turku, Finland, 2016.
[22] T.N. Pham, Three-dimensional Structured Carbon Foam: Synthesis and Applications, Umeå University, Umeå, Sweden, 978-91-7601-574-2, 2016.
[23] L.J. Konwar, Y. Sugano, R.S. Chutia, P. Mäki-Arvela, R. Kataki, J.-P. Mikkola, Mater. Lett. 173 (2016) 145–148.
[24] L.J. Konwar, P. Mäki-Arvela, E. Salminen, N. Kumar, A.J. Thakur, J.-P. Mikkola, D. Deka, Appl. Catal. B: Environ. 176–177 (2015) 20–35.
[25] T.N. Pham, T. Sharifi, R. Sandström, W. Siljebo, A. Shchukarev, K. Kordas, T. Wågberg, J.-P. Mikkola, Sci. Rep. 7 (2017) 6112.
[26] P.J.F. Harris, Z. Liu, K. Suenaga, J. Phys. Conf. Ser. 241 (2010) 012–050.
[27] D. Guo, R. Shibuya, C. Akiba, S. Saji, T. Kondo, J. Nakamura, Science 351 (6271) (2016) 361–365.
[28] B. Li, X. Sun, D. Su, Phys. Chem. Chem. Phys. 17 (2015) 6691–6694.
[29] A. Dandekar, R.T.K. Baker, M.A. Vannice, Carbon 36 (1998) 1821–1831.
[30] A.I. Adeleye, D. Patel, D. Niyogi, B. Saha, Ind. Eng. Chem. Res. 53 (49) (2014) 18647–18657.
[31] L.J. Konwar, J. Wärnå, P. Mäki-Arvela, N. Kumar, J.-P. Mikkola, Fuel 166 (2016)

1–11.
[32] J. Kim, S.N. Kim, H.G. Jang, G. Seo, W.S. Ahn, Appl. Catal. A Gen. 453 (2013) 175–180.
[33] A.H. Chughtai, N. Ahmad, H.A. Younus, A. Laypkov, F. Verpoort, Chem. Soc. Rev. 44 (2015) 6804–6849.
[34] S. Dutta, A. Bohre, W. Zheng, G.R. Jenness, M. Núñez, B. Saha, D.G. Vlachos, ACS Catal. 7 (2017) 3905–3915.
[35] L.J. Konwar, A. Samikannu, P. Mäki-Arvela, J.-P. Mikkola, Catal. Sci. Technol. 8 (2018) 2449–2459.
[36] I. Ogino, Y. Suzuki, S.R. Mukai, Catal. Today 314 (2018) 62–69.